Optical Engineering

OpticalEngineering.SPIEDigitalLibrary.org

Resolving multiple propagation paths in time of flight range cameras using direct and global separation methods

Refael Whyte
Lee Streeter
Michael J. Cree
Adrian A. Dorrington

SPIE.

Resolving multiple propagation paths in time of flight range cameras using direct and global separation methods

Refael Whyte,* Lee Streeter, Michael J. Cree, and Adrian A. Dorrington
University of Waikato, School of Engineering, Private Bag 3105, Hamilton 3240, New Zealand

Abstract. Time of flight (ToF) range cameras illuminate the scene with an amplitude-modulated continuous wave light source and measure the returning modulation envelopes: phase and amplitude. The phase change of the modulation envelope encodes the distance travelled. This technology suffers from measurement errors caused by multiple propagation paths from the light source to the receiving pixel. The multiple paths can be represented as the summation of a direct return, which is the return from the shortest path length, and a global return, which includes all other returns. We develop the use of a sinusoidal pattern from which a closed form solution for the direct and global returns can be computed in nine frames with the constraint that the global return is a spatially lower frequency than the illuminated pattern. In a demonstration on a scene constructed to have strong multipath interference, we find the direct return is not significantly different from the ground truth in 33/136 pixels tested; where for the full-field measurement, it is significantly different for every pixel tested. The variance in the estimated direct phase and amplitude increases by a factor of eight compared with the standard time of flight range camera technique. [DOI: 10.1117/1.OE.54.11.113109]

Keywords: time of flight imaging; multipath interference; direct/global separation; range imaging.

Paper 150998 received Jul. 22, 2015; accepted for publication Oct. 26, 2015; published online Nov. 24, 2015.

1 Introduction

Range imaging is a growing area with applications in machine vision, human computer interaction, and manufacturing. Time of flight (ToF) range cameras measure distance by illuminating the scene with an amplitude-modulated continuous wave light source. Typically, the frequency of the amplitude modulation is in the megahertz range. The emitted light travels to the objects in the scene and reflects back to the imaging sensor, and the distance the light has travelled is encoded as a phase shift in the amplitude modulation envelope. Each pixel of the imaging sensor measures this phase shift for the returning light. Multiple propagation paths from the light source to the same pixel cause measurement errors, and typically arise from inter-reflections, lens flare, subsurface scattering, volumetric scattering, and translucent surfaces. The error caused by multiple propagation paths is called multipath interference and is a major source of error in ToF range cameras.[1] Multipath interference is highly scene dependent adding to the complexity of a solution.

Previous work on resolving multipath interference in ToF range cameras includes using multiple modulation frequencies, sparse deconvolution, and solving optimization problems. The relationship between phase and modulation frequency is nonlinear when multipath interference is present. Dorrington et al.[2] resolved multipath interference using measurements at two different modulation frequencies. This work was expanded by Godbaz et al.[3] to a closed form solution by using four modulation frequencies. Bhandari et al.[4] and Kirmani et al.[5] later generalized the solution to five or more modulation frequencies. Part of the measurement in ToF cameras is the correlation between the returning optical signal and a reference signal. Use of sparse deconvolution on the correlation signal to solve multipath interference was shown by Godbaz et al.[6] This was expanded by Kadambi et al.[7] by using binary sequences to increase the spectral content of the correlation signal and improve the sparse deconvolution. Fuchs et al.[8] and Jiménez et al.[9] both posed iterative optimization problems constrained by the measured data to estimate the multipath interference. Both of these authors assume the only mode of multipath interference is inter-reflections in the scene.

Decomposition of the light transport into multiple bounces was shown by Setiz et al.[10] The light transport was broken into a direct component and M returns. This was developed into dual photography, where the viewpoint between a projector and camera could be interchanged.[11] The theory of light transport was developed into two return components, the direct return which is the shortest path length, and the global return which contains everything else. Nayar et al.[12] demonstrated a fast method for separating the direct return and global components by illuminating the scene with a checkerboard (CB) pattern and by phase shifting the pattern. The direct and global components can be recovered if the spatial frequency of the global return is much lower than the spatial frequency of the projected pattern. Global components of light propagation also cause issues for structured light range measurement techniques. The development of structured light patterns to remove the global

*Address all correspondence to: Refael Whyte, E-mail: rzw2@students.waikato.ac.nz

0091-3286/2015/$25.00

effects has been an area of research.[13,14] Using direct time of flight range measurements to perform light transport analysis was performed by Wu et al.[15] Their method relied on the direct measurement of the flight time of light; therefore, the multipath interference problem was trivial to solve. O'Toole et al.[16] applied direct and global separation to ToF range cameras for transient imaging. Recently, Naik et al.[17] used a CB pattern with a ToF range camera. They compared the result to the ground truth measurements performed with a line scanner.

In this paper, direct and global separation is adapted to ToF camera operation. ToF cameras measure the phase and amplitude of the returning light, while conventional cameras measure the intensity of the light in the scene. Therefore, current techniques for measuring direct and global components need to be modified for use in ToF range cameras. The modified technique is used to recover the phase and amplitude of the direct and global components, thereby correcting the errors caused by multipath interference. An illumination pattern is presented that is optimized for minimizing the number of frames required to resolve the direct and global components.

2 Theory

In this section, we review the theory of ToF range camera operation and the background of direct global separation. Then we adapt and combine the two techniques such that the direct and global components are separated using Fourier analysis.

2.1 *Time of Flight Range Camera Operation*

ToF range cameras illuminate the scene with amplitude modulated light. The phase shift between the transmitted modulation envelope and the reflection from the scene encodes the distance the light has travelled. The reflected light can be expressed as

$$s(t) = a\ \sin(\omega_r t - \phi) + b, \tag{1}$$

where a is the amplitude of the returning light, ω_r is the angular modulation frequency, ϕ is the phase offset due to the distance travelled, and b is the background light. The phase offset due to distance travelled d is defined as

$$\phi = \frac{4\pi d f_r}{c}, \tag{2}$$

where c is the speed of light. To extract the phase, the reflected light is correlated by a reference signal $g(t)$

$$g(t) = \sin(\omega_r t). \tag{3}$$

The correlation signal, $h(\tau)$, is measured at each pixel, where $h(\tau)$ is the correlation between Eq. (1) and Eq. (3)

$$h(\tau) = (s \star g)(t) = \frac{1}{T} \lim_{T\to\infty} \int_{-T/2}^{T/2} s(t) \cdot g(t+\tau)\, \mathrm{d}t, \tag{4}$$

where τ is the phase of the reference waveform $g(t)$. Evaluation of the integral in Eq. (4) yields

$$h(\tau) = \frac{a}{2}\ \cos(\omega_r \tau + \phi) + b. \tag{5}$$

Multiple measurements are taken on the correlation signal by phase shifting the reference signal. A minimum of three measurements are required, four are typically used.[18] To demodulate, the discrete Fourier transform (DFT) is taken on $h(\tau)$ and the first order bin contains the amplitude and phase. Ideally, the measured phase and amplitude can be expressed as a complex exponential

$$\zeta = a\ \exp(-j\phi). \tag{6}$$

In reality, when multipath interference is present in the measurement, the problem can be expressed as the sum of M complex exponentials such that

$$\zeta = \sum_{m=1}^{M} a_m\ \exp(-j\phi_m). \tag{7}$$

In the case of one propagation path, $M = 1$, then Eq. (7) simplifies to Eq. (6). Resolving multipath interference is difficult because there are an infinite number of combinations that sum to the measured value. The propagation of light can be represented by the direct and global components. The return with the shortest path length is the direct component, and the global return encompasses all other returns. Figure 1 shows an example of multiple propagation paths in a corner caused by inter-reflections.

2.2 *Direct and Global Component Separation*

Direct and global separation decomposes the measured radiance, L, at each pixel into a direct component L_d and a global component L_g[12]

$$L = L_d + L_g. \tag{8}$$

2.2.1 *Checkerboard illumination pattern*

Consider illumination by a CB pattern so that half the scene is dark and the other half illuminated. In the illuminated pixels, the measured signal is[12]

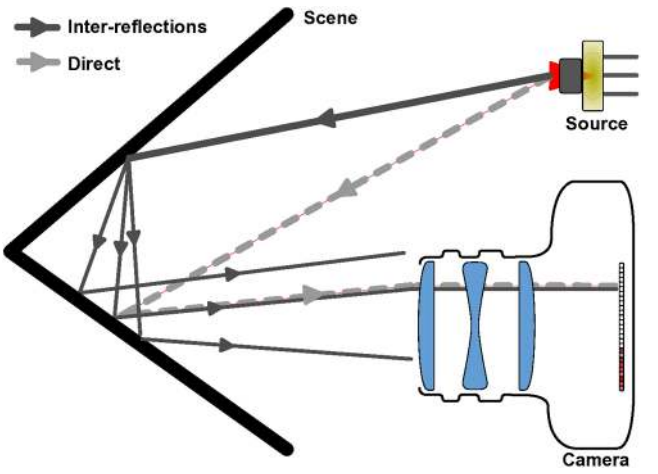

Fig. 1 The measured signal of one pixel is due to the direct illumination from the source and the global illumination. The global illumination can be caused by inter-reflections as shown, subsurface scattering, volumetric scattering, and translucency.

$$L_{\max} = L_d + \frac{1}{2}L_g. \tag{9}$$

The assumption is the global component is at a lower spatial frequency than the pattern. Half the scene is illuminated with a CB pattern, therefore, half the global component is present. When illuminated with the inverse CB pattern the bright pixels become dark pixels at which the camera measures

$$L_{\min} = \frac{1}{2}L_g. \tag{10}$$

This set of two equations is well posed, and the inversion is

$$L_g = 2L_{\min}, \tag{11}$$

$$L_d = L_{\max} - L_{\min}. \tag{12}$$

Nayar et al.[12] proposed shifting the CB pattern five shifts in the x direction for each five shifts in the y direction giving 25 acquisitions.

2.2.2 *Sinusoidal illumination pattern*

In this section, we review direct and global separation using sinusoidal (SW) illumination patterns allowing for separation with three raw frames.[12] The scene is illuminated with a spatially varying pattern according to the following function

$$P(x,y) = \frac{A}{2}\left\{1 + \sin\left[\frac{2\pi x}{p} + \upsilon + \sin\left(\frac{2\pi y}{q}\right)\right]\right\}, \tag{13}$$

where P is the projected image, x and y are the projector coordinates, and υ is the phase shift of the pattern in pixels per frame (time) in the x dimension. The variables p and q change the frequency of the pattern in the x and y directions, respectively, and the light source has a maximum amplitude A. To perform separation, the pattern is phase shifted in the x direction between frames, making υ a function of time t, where $\upsilon(t) = \omega_p t$. The radiance each pixel measures over time (each frame) is

$$L(t) = \frac{A \cdot [1 + \sin(\omega_p t + \theta)]}{2}, \tag{14}$$

where θ is the phase offset of the projected pattern defined by $\theta = 2\pi x/p + \sin(2\pi y/q)$. Since the global return is spatially smooth, its contribution to the radiance is constant between projected images, therefore, it is constant with time. The measured radiance over time is, therefore

$$I(t) = L_d\frac{[1 + \sin(\omega_p t + \theta)]}{2} + \frac{L_g}{2}, \tag{15}$$

$$= \frac{L_d}{2}\sin(\omega_p t + \theta) + \frac{L_d + L_g}{2}. \tag{16}$$

By expansion of the trigonometric functions and rearrangement, Eq. (16) becomes

$$I(t) = \eta\sin(\omega_p t) + \beta\cdot\cos(\omega_p t) + \frac{1}{\sqrt{2}}\gamma, \tag{17}$$

where

$$\eta = L_d\cos(\theta)/2, \tag{18}$$

$$\beta = L_d\sin(\theta)/2, \tag{19}$$

$$\gamma = \frac{(L_d + L_g)}{\sqrt{2}}. \tag{20}$$

The unknowns η, β, γ can be extracted by taking the DFT over t. The direct and global components are calculated by

$$L_d = 2\sqrt{\eta^2 + \beta^2}, \tag{21}$$

$$L_g = \sqrt{2}\gamma - L_d. \tag{22}$$

3 Combination of Time of Flight with Direct and Global Separation

This section describes the theory of resolving the direct and global components in ToF range images by combining the spatially varying illumination patterns with the phase shifting signal in ToF imaging. Both CB and SW patterns are analyzed.

The multipath interference problem from Eq. (7) can be written in terms of the direct and global components

$$\zeta = a_d\exp(-j\phi_d) + a_g\exp(-j\phi_g) = L_d + L_g, \tag{23}$$

where

$$L_d = a_d\exp(-j\phi_d), \tag{24}$$

$$L_g = a_g\exp(-j\phi_g). \tag{25}$$

a_d and ϕ_d are the amplitude and phase of the direct component, respectively, and a_g and ϕ_g are the amplitude and phase of the global component. With ToF range cameras, L_d and L_g are complex numbers, therefore, destructive interference can occur. It is assumed that there is one direct return which is the shortest return from the light source to the pixel and a global return which includes all other returns.

When using a high frequency CB pattern as the illumination source, Eqs. (9)–(12) can still be used with complex components if certain assumptions are made. The maximum and minimum values are estimated by the amplitude of the complex measurement

$$L_{\max\_est} \simeq \max|L(t)| = |\zeta| = \sqrt{a_d^2 + a_g^2 + 2a_d a_g\cos(-\phi_d - \phi_g)}, \tag{26}$$

$$L_{\min\_est} \simeq \min|L(t)| = a_g. \tag{27}$$

This approximation is valid provided that

$$L_{\max\_est} > L_{\min\_est} \Rightarrow |L_g + L_d| > |L_g|. \tag{28}$$

The constraint from Eq. (28) is always satisfied when either

$$2|L_g| < |L_d|, \tag{29}$$

or

$$|\phi_g - \phi_d| \leq \pi/2, \tag{30}$$

holds. To illustrate Eq. (28), note that the direct and global components add on the complex plane; therefore, in some situations, the amplitude of the sum can be less than the individual amplitudes. For Eqs. (27) and (26), in order to remain valid approximations, either the amplitude of the direct has to be much greater than the amplitude of the global, [Eq. (29)] or the phase difference has to be less than $\pi/2$ for constructive interference, giving rise to Eq. (30). In other words, to determine the direct and global returns, the amplitude of the direct plus global must always be larger than the amplitude of just the global illumination, see Fig. 2.

Separation with no constraints and the minimum number of frames is desired. The constraints inherent with using CB illumination patterns are undesirable, and we seek separation of direct and global with no such constraints and, thus a minimum number of frames. The general form can be expressed as the combination of Eqs. 15 and (5). This leads to

$$I(t,\tau) = \frac{h_d(\tau)}{2} \cdot L(t) + \frac{h_g(\tau)}{2}, \tag{31}$$

where h_d and h_g are the correlation waveforms for the direct and global components and $L(t)$ is the projected pattern that changes with time. $L(t)$ can describe any projected pattern that is phase shifted with time, such as an SW or square wave pattern. Using multiple modulation, frequencies can be included in the above equation, and the resulting equations become

$$\phi(\omega_r) = \frac{2\omega_r d}{c}, \tag{32}$$

$$h(\tau,\omega_r) = \frac{a}{2}\cos[\omega_r\tau + \phi(\omega_r)], \tag{33}$$

$$I(t,\tau,\omega_r) = \frac{h_d(\tau,\omega_r)}{2} \cdot L(t) + \frac{h_g(\tau,\omega_r)}{2}. \tag{34}$$

We propose a function $L(t)$ to facilitate separation of the direct and global under Fourier analysis.

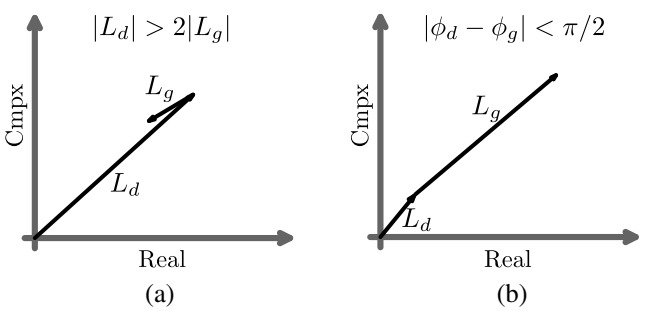

Fig. 2 The constraints from Eqs. (29) and (30) are visualized on the complex plan in (a) and (b), respectively. The amplitude of the result of $L_d + L_g$ must always be greater than the amplitude of L_g for the approximation in Eqs. (26) and (27) to be true.

Let $L(t)$ be a cosine wave by projecting the high frequency spatial SW pattern from Eq. 14 and frequency such that

$$L(t) = \frac{1 + \cos(\omega_p t - \theta)}{2}, \tag{35}$$

$$\omega_p t = l\omega_r\tau, \tag{36}$$

where l is a positive integer. Then the combination of Eqs. (31) and (35) becomes

$$\begin{aligned} I(\tau) = \frac{a_d}{4}\{&\cos[(l-1)\omega_r\tau + \theta - \phi_d] \\ &+ \cos[(l+1)\omega_r\tau + \theta + \phi_d]\} \\ &+ \frac{a_d\cos(\omega_r\tau + \phi_d) + a_g\cos(\omega_r\tau + \phi_g)}{2}. \end{aligned} \tag{37}$$

With $l = 3$, a closed form solution is present with the fewest samples. With α_k and φ_k being the amplitude and phase at the k^{th} Fourier frequency and $l \geq 3$ then

$$\theta = \frac{\varphi_{l-1} + \varphi_{l+1}}{2}, \tag{38}$$

$$\phi_d = \frac{\varphi_{l+1} - \varphi_{l-1}}{2}, \tag{39}$$

$$a_d = 2(\alpha_{l-1} + \alpha_{l+1}), \tag{40}$$

$$\frac{a_g}{2}\exp(-j\phi_g) = \alpha_1\exp(-j\varphi_1) - \frac{a_d}{2}\exp(-j\phi_d). \tag{41}$$

There are no constraints on the direct and global components in addition to the fundamental constraint that the global component is bandlimited in the spatial Fourier domain. In Table 1, we enumerate for integer values of l if the problem is solvable using Fourier analysis and the number of samples is required in time.

3.1 *Harmonic Error Analysis*

The above analysis ignores the well recognized fact that unwanted harmonics add error to ToF ranging.[19] These unwanted harmonics arise from the common hardware implementation that utilizes square wave modulation driven by digital circuitry. The correlation signal is, therefore, a triangle waveform and higher order odd harmonics are present in the signal. The addition of the odd harmonics has the following effect:

Table 1 Summary of solvability of Eq. (37) using Fourier analysis for different values of *l*. The number of samples is calculated by the Nyquist frequency.

l	0	1	2	3	4	5
Solvable	No	No	No	Yes	Yes	Yes
Samples	—	—	—	9	11	13

$$h(\tau) = \sum_{k=1,3,5,\ldots}^{K} \frac{a}{2k^2} \cos(k\omega_r \tau + k\phi), \tag{42}$$

and

$$I(\tau) = \left[\sum_{k=1,3,\ldots}^{K} \frac{a_d}{2\,k^2} \cos(k\omega_r \tau + k\phi_d)\right] \cos(l\omega_r \tau - \theta) + \frac{h_g(\tau) + h_d(\tau)}{2}, \tag{43}$$

$$= \frac{h_g(\tau) + h_d(\tau)}{2} + \sum_{k=1,3,\ldots}^{K} \left\{ \frac{a_d}{4k^2} \cos[(k+l)\omega_r \tau + k\phi_d - \theta] + \frac{a_d}{4k^2} \cos[(k-l)\omega_r - k\phi_d - \theta)] \right\}. \tag{44}$$

In the case where nine samples are used, the third harmonic of the triangular modulation signal is mixed onto the zeroth and sixth harmonic. Then the sixth harmonic is aliased onto the third harmonic, which is not used to compute the direct component. However, the fifth harmonic is mixed onto the second and eighth harmonics. In addition, the eighth harmonic is aliased onto the first harmonic, which causes errors in the direct and global computation. The presence of the third harmonic does not cause problems but the fifth does.

3.2 *Propagation of Uncertainty*

Each measurement of the correlation function is affected by noise. In time of flight cameras, this consists of photon shot noise, dark current, ADC quantization, and jitter. It is assumed that the resulting noise is white and independent between samples. Schoukens and Renneboog[20] showed if these conditions are met then the scaled covariance matrix C for the DFT is

$$C = \frac{2}{N} \sigma_{h_\tau}^2 I, \tag{45}$$

where N is the number of samples, I is the identity matrix, and $\sigma_{h_\tau}^2$ is the variance of the additive white noise.

Assuming the real and imaginary components are independent, then the variance of the amplitude a and phase ϕ for each Fourier bin is

$$\sigma_a^2 = \frac{1}{N} \sigma_{h_\tau}^2, \tag{46}$$

$$\sigma_\phi^2 = \frac{2}{Na^2} \sigma_{h_\tau}^2. \tag{47}$$

Equations (46) and (47) are the generalization from four samples, given by Frank et al.,[21] to N samples. Due to the mixing of the described technique, the amplitude of the Fourier bins compared with the standard ToF measurement is

$$\alpha_{l-1} = \alpha_{l+1} \approx \frac{a}{4}, \tag{48}$$

then the variance compared with the total can be computed as

$$\sigma_{a_d}^2 = \frac{8}{N} \sigma_{h_\tau}^2, \tag{49}$$

$$\sigma_{\phi_d}^2 = \frac{16}{Na_t^2} \sigma_{h_\tau}^2. \tag{50}$$

The variance of the direct phase and amplitude estimation increases by eight times compared with using the standard time of flight technique. The variance in the global component is greater because the global is calculated from the direct.

4 Hardware and Experimentation

A custom built ToF range camera designed to implement direct and global separation is used for the experimentation. The camera is built around a PMD19k3 (PMD Technologies, Siegen, Germany) sensor which contains a 120×160 pixel array, and is based on the reference design by Jongenelen et al.[22] The PMD19k3 sensor is controlled by a Cyclone IV FPGA (Altera, San Jose, California). The analog pixel values are converted to 16 bit unsigned values by an AD9862 ADC (Analog Devices, Norwood, Massachusetts), and images are then transmitted to the host computer over Ethernet.

A DLP LightCrafter (Texas Instruments, Dallas, Texas) projector was modified to illuminate the scene with the desired patterns. The LEDs from the projector are removed and the red LED was replaced with a HL6545MG (Opnext, Nagano, Japan) 660 nm 120 mW laser diode. The laser diode is controlled by the camera and both are amplitude modulated at 30 MHz. The projector was calibrated to have a linear amplitude response.

The projector's field of view is different from the camera due to the manufacturer's supplied optics. Therefore, some parts of the scene viewed by the camera are not illuminated by the projector. In the occlusions and nonilluminated regions, no direct return should be present, therefore, the computed phase is invalid. In some cases, phase values are removed if the amplitude is below a fixed threshold.

A variety of scenes were imaged to test the performance of the proposed direct and global separation method. Each scene was designed with material selection and scene preparation, so that one form of multipath interference is more dominantly present than other forms. The scenes include an internal corner, which emphasizes inter-reflections between surfaces; wax and peppers, which is dominated by subsurface scattering; and the CB, which highlights lens flare. For each scene, both the CB and SW direct and global separation methods are used. The CB method requires 100 raw frames, which provides 25 depth frames, and the SW method uses nine raw frames.

To test the accuracy of the direct and global separation on complex data, the ground truth distance is required. To acquire the ground truth of the internal corner, each side is illuminated with small patches with the opposing side removed. The illumination of small patches and the removal of scattering objects means that we can assume that the measured return is the direct return. The purpose of this test is to

demonstrate that the direct measurements are more accurate than the full field (FF) and to statistically present it. The average of 100 ground truth phase images is computed to obtain a single reference image. The reference image is subtracted from each of the one hundred FF, CB, and the SW phase images. The root mean squared error (RMSE) is calculated for the phase of each of the FF, CB, and SW methods. The mean and standard deviations of the 100 RMSE values for each method are then tabulated for comparison of the RMSEs between the methods. Significance testing is performed by the Wilcoxon signed rank paired test for difference in the median of the RMSE between the different methods.

To test the proposed method on a specular corner to examine the effect of nonspatially smooth global illumination, a right angle corner is constructed with one side from a metallic cake tin and the other side with white diffuse foam board. The ground truth is measured by illuminating small patches separately so only the direct return is present in the patch. The ground truth distance is compared against the direct and global separation and FF illumination distance measurements.

The direct and global separation is compared with the methods for resolving multipath interference by Kadambi et al.[7] and Bhandari et al.[4] A right angle corner is constructed out of white foam board and the camera is located 1.0 m away and 0.37 m up from the corner point and looks down upon the corner at 20 degrees. The binary sequence used for the Kadambi method is a 31 bit maximum length sequence generated with a bit time of 20 ns (50 MHz) and 4960 measurements are taken on the cross-correlation signal. Five modulation frequencies are used for the Bhandari method: they are 10, 20, 30, 40, and 50 MHz, and at each frequency, 16 phase steps are taken. The ground truth of one column of pixels is captured by raster scanning a small patch of direct illumination. The RMSE of one column is calculated for each depth frame, and 100 depth frames of each method are measured, then the RMSE mean and standard deviation of each method is tabulated.

5 Results and Discussion

5.1 *Corner*

In Fig. 3, we compare the measured phase of one row in the corner when using FF illumination, the recovered direct distance component, and the ground truth distance measurement. The direct component is consistent with the ground truth and they align within three standard deviations of each other. The measured phase in the corner when using FF illumination is consistent with results shown by Fuchs.[23]

The mean and standard deviation of the phase RMSE over 100 frames for the three measurement techniques is tabulated in Table 2. Each RMS value reported is separated by more than three standard deviations. The result of the Wilcoxon signed rank test between FF and CB illumination, and between CB and SW illumination, both have p-values that are zero to machine precision, which supports the assertion that the direct and global separation are successful.

5.2 *Peppers and Wax*

The results of the direct and global separation on a group of peppers and wax candles are presented in Fig. 4. The

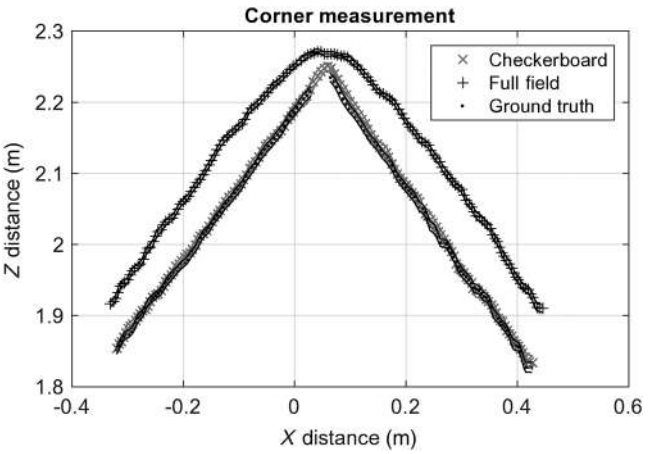

Fig. 3 Comparison of the measured phase when using full-field illumination and the reconstructed direct component using checkerboard (CB) patterns compared with the ground truth, with plus and minus three standard deviations plotted around each measurement.

amplitude of the global component shows significant subsurface scattering in the peppers and the wax. There are interreflections between the objects and the table top and interreflections between the base and wall. The wavelength of the light source is 660 nm (red); therefore, the red and yellow peppers are brighter than the green peppers. There is a significant difference between the candles' distances in Figs 4(b) and 4(c), and the peppers are at different distances. In Fig. 4(b), the peppers' distance is related to the measured amplitude, and brighter parts of the peppers are closer, while in Fig. 4(c), the peppers' distance is not related to brightness, indicating that multipath interference caused by subsurface scattering is removed by direct and global separation.

5.3 *Color Dependence*

Figure 5 shows the results of the direct and global separation of a black and white CB on a flat sheet. The SW pattern and CB pattern correct the phase error seen in the FF image. Lindner et al.[24] demonstrated a distance error correlated with amplitude and attempted a correction with calibration. Lichti et al.[25] also used scattering models to perform depth calibration based on amplitude. This result shows the distance error with amplitude in ToF range cameras is due to multipath interference, probably caused by lens flare, and can be corrected with direct and global separation.

5.4 *Specular Corner*

Figure 6 demonstrates that the inter-reflections caused by the cake tin are not diffuse, and therefore, violate the assumption of a spatially smooth global component. The measured

Table 2 Mean and standard deviation of phase RMSE over 100 frames for full field (FF), checkerboard (CB), and sinusoidal (SW) illumination techniques.

	FF	CB	SW
RMSE Mean	0.0952	0.0153	0.0112
RMSE STD	0.58×10^{-3}	0.11×10^{-3}	0.16×10^{-3}

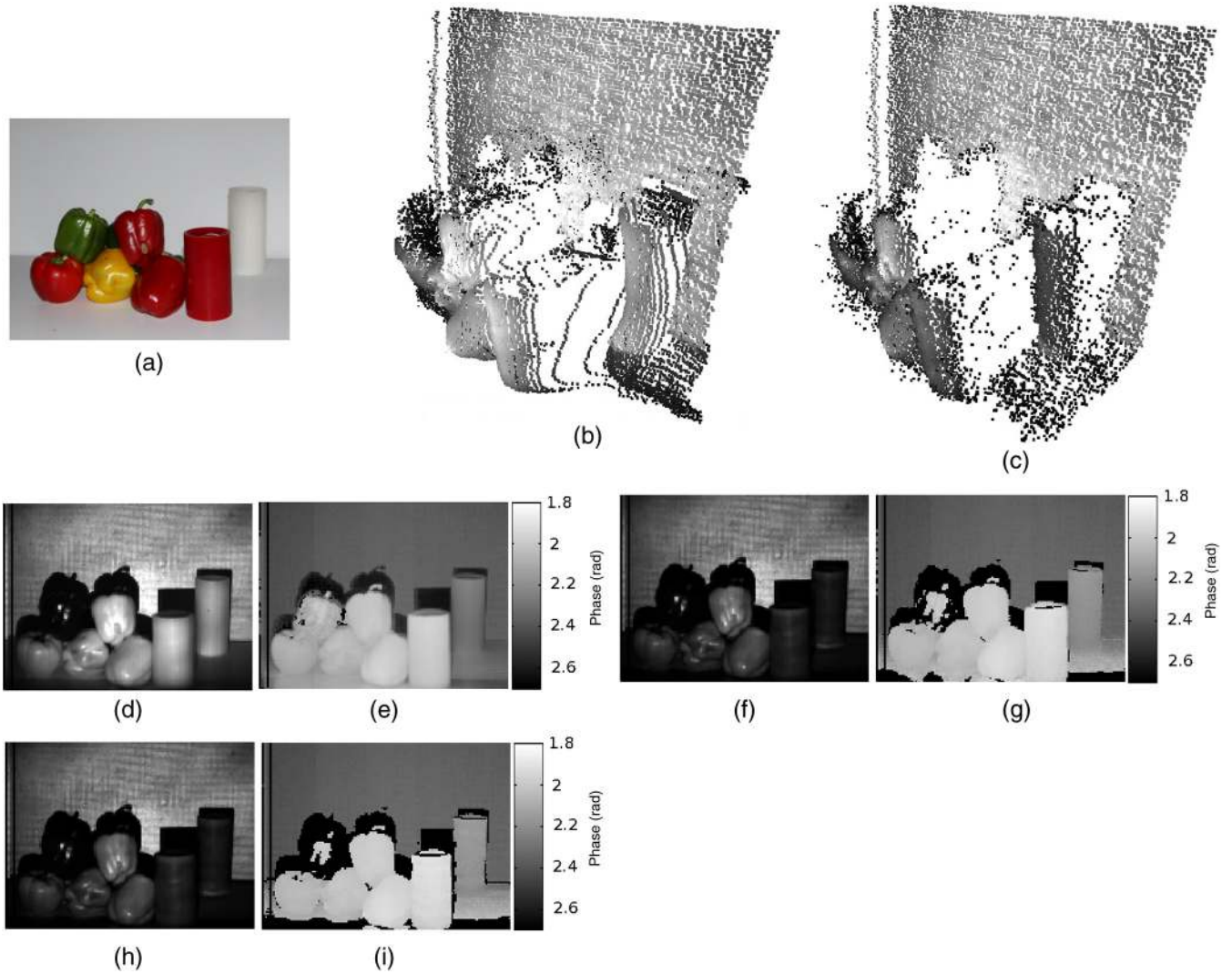

Fig. 4 The direct and global components from subsurface scattering in wax candles and peppers and inter-reflections on the white floor and wall: (a) scene photo, (b) full-field (FF) point cloud, (c) CB direct point cloud, (d) FF amplitude, (e) FF phase, (f) CB direct amplitude, (g) CB direct phase, (h) sinusoidal (SW) direct amplitude, and (i) SW direct phase.

distance along the slice in Fig. 6(a) is plotted in Fig. 7 for the ground truth distance, FF distance, and the direct distance. The RMSE for the FF distance slice is 0.0601, while for the direct distance it is 0.0435. The error has been reduced compared with FF; however, significant error still exists as predicted above in Sec. 2.

5.5 *Comparison With Other Methods*

The presented method fails on specular reflections because they violate the global spatial frequency constraint, as demonstrated in Fig. 7. The direct and global separation for resolving multipath interference is compared with methods presented by Kadambi et al.[7] and Bhandari et al.[4] for resolving multipath interference in a diffuse corner for one column of pixels. The RMSE of each method and the RMSE standard deviation over 100 frames is tabulated in Table 3. The RMSE for Kadambi et al.[7] is greater than FF in the corner, which is due to the depth quantization caused by the method. The RMSE is reduced less than FF for the method presented by Bhandari et al.,[4] but the reduction of error is small compared with the presented direct and global separation. The forward models presented by Kadambi et al.[7] and Bhandari et al.[4] both assume a sparse number of returns, which is not the case for a diffuse corner; therefore, they fail to resolve the corner, while the direct and global separation significantly reduces the measurement error.

The presented method requires nine raw frames for a closed form solution to resolve multipath interference. The previous closed form solution by Godbaz et al.[3] required phase and amplitude at four different frequencies, thus the minimum number of raw frames would be 12. In contrast, Kadambi et al.[7] used 3000 raw frames. Previous work by Dorrington et al.[2] used two frequencies for a minimum of 6 raw frames, however, was not a closed form solution.

Recently, Naik et al.[17] have used a CB pattern with a ToF range camera. They compared the result to the ground truth measurements performed with a line scanner. We have developed further constraints for using CB patterns and expanded direct and global separation to mix the ToF signal with an

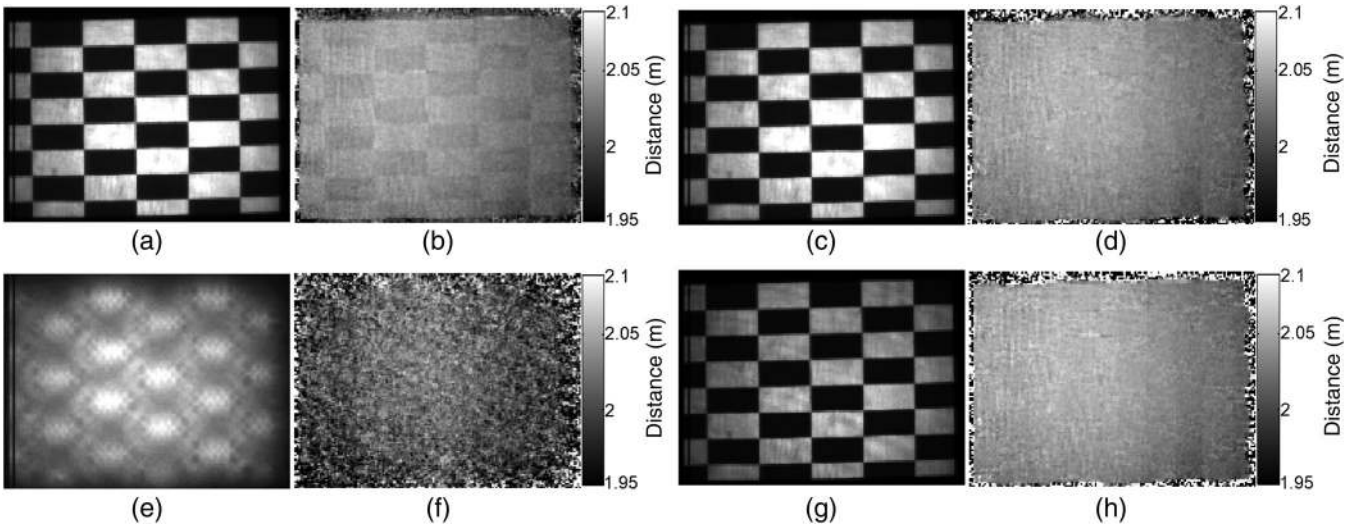

Fig. 5 Results of using direct and global separation to correct for distance error due to different reflectivity. The results are for CB and SW patterns. The depth in (b) is correlated with the amplitude in (a). In (d) and (h), the depth is not correlated with the amplitude: (a) FF amplitude, (b) FF phase, (c) CB amplitude, (d) CB direct phase, (e) CB global, (f) CB global phase, (g) SW amplitude, and (h) SW phase.

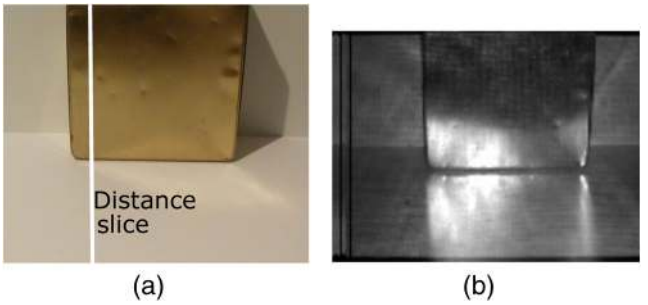

Fig. 6 Photo of corner created with a cake tin in (a), and the measured amplitude with a full field time of flight range camera in (b). The cake tin reflection is highly visible in the amplitude image.

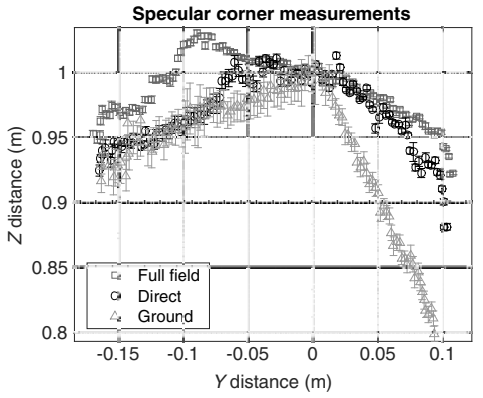

Fig. 7 The measured distance for FF illumination and direct and global separation compared with the ground truth for the corner pictured in Fig. 6(a). The error bars are plus and minus one standard deviation. At the top of the cake tin, the direct and global separation reduces the distance error as the global return is diffuse, while for the rest of the distance slice, the error is not reduced as the global return is not spatially smooth.

Table 3 Comparison of root mean square error (RMSE) for FF illumination and three methods of resolving multipath interference in a corner for one column, Kadambi et al.,[7] Bhandari et al.,[4] and our presented method.

	FF	Kadambi et al.[7]	Bhandari et al.[4]	Direct
RMSE mean	0.0267	0.0299	0.0217	0.0085
RMSE STD	1.24×10^{-3}	0.41×10^{-3}	0.83×10^{-3}	0.25×10^{-3}

SW pattern for a closed form solution under Fourier analysis in nine raw frames.

Previous methods for resolving measurement errors due to lens flare rely on calibration[24] and estimating the complex point spread function[9] of the mixing in the lens. With the presented method, no calibration is required; therefore, no assumptions are made about the scene.

6 Conclusion

ToF range cameras suffer from measurement errors caused by multiple propagation paths. We have demonstrated the use of CB direct and global separation but have also exposed a limitation in the use of a CB pattern in the form of constraints on the values that the direct and global complex phasors can take. We also have developed a method of combining the phase measurement of ToF cameras and SW patterns used in direct and global serration. The method has a closed form solution requiring nine raw frames. Using the direct and global separation, the correct distance was measured for a corner, and qualitatively demonstrated removal of subsurface scattering and artifacts caused by lens scattering.

References

1. S. Guomundsson, H. Aanaes, and R. Larsen, "Environmental effects on measurement uncertainties of time-of-flight cameras," in *Int. Symp. on Signals, Circuits and Systems (ISSCS)*, Vol. 1, pp. 1–4 (2007).

2. A. A. Dorrington et al., "Separating true range measurements from multi-path and scattering interference in commercial range cameras," *Proc. SPIE* **7864**, 4–10 (2011).
3. J. P. Godbaz et al., "Closed-form inverses for the mixed pixel/multi-path interference problem in AMCW lidar," *Proc. SPIE* **8296**, 829618 (2012).
4. A. Bhandari et al., "Resolving multipath interference in time-of-flight imaging via modulation frequency diversity and sparse regularization," *Opt. Lett.* **39**, 1705–1708 (2014).
5. A. Kirmani, A. Benedetti, and P. Chou, "SPUMIC: Simultaneous phase unwrapping and multipath interference cancellation in time-of-flight cameras using spectral methods," in *IEEE Int. Conf. on Multimedia and Expo (ICME)*, pp. 1–6 (2013).
6. J. Godbaz, M. Cree, and A. Dorrington, "Mixed pixel return separation for a full-field ranger," in *23rd Int. Conf. on Image and Vision Computing New Zealand (IVCNZ)*, pp. 1–6 (2008).
7. A. Kadambi et al., "Coded time of flight cameras: Sparse deconvolution to address multipath interference and recover time profiles," *ACM Trans. Graph.* **32**, 1–10 (2013).
8. S. Fuchs, M. Suppa, and O. Hellwich, "Compensation for multipath in ToF camera measurements supported by photometric calibration and environment integration," *Lec. Notes Comput. Sci.* **7963**, 31–41 (2013).
9. D. Jiménez et al., "Modeling and correction of multipath interference in time of flight cameras," *Image Vision Comput.* **32**(1), 1–13 (2014).
10. S. Seitz, Y. Matsushita, and K. Kutulakos, "A theory of inverse light transport," in *10th IEEE Int. Conf. on Computer Vision (ICCV)*, Vol. 2, pp. 1440–1447 (2005).
11. P. Sen et al., "Dual photography," *ACM Trans. Graph.* **24**(3), 745–755 (2005).
12. S. K. Nayar et al., "Fast separation of direct and global components of a scene using high frequency illumination," *ACM Trans. Graph.* **25**, 935–944 (2006).
13. M. Gupta et al., "A practical approach to 3D scanning in the presence of interreflections, subsurface scattering and defocus," *Int. J. Comput. Vision* **102**(1-3), 33–55 (2013).
14. J. Gu et al., "Multiplexed illumination for scene recovery in the presence of global illumination," in *IEEE Int. Conf. on Computer Vision (ICCV)*, pp. 691–698 (2011).
15. D. Wu et al., "Decomposing global light transport using time of flight imaging," *Int. J. Comput. Vision* **107**(2), 123–138 (2014).
16. M. O'Toole et al., "Temporal frequency probing for 5D transient analysis of global light transport," *ACM Trans. Graph.* **33**, 87:1–87:11 (2014).
17. N. Naik et al., "A light transport model for mitigating multipath interference in time-of-flight sensors," in *Proc. IEEE Conf. on Computer Vision and Pattern Recognition*, pp. 73–81 (2015).
18. R. Lange, "3D time-of-flight distance measurement with custom solid-state image sensors in CMOS/CCD-technology," PhD Thesis, University of Siegen (2006).
19. A. D. Payne et al., "Improved linearity using harmonic error rejection in a full-field range imaging system," *Proc. SPIE* **6805**, 68050D (2008).
20. J. Schoukens and J. Renneboog, "Modeling the noise influence on the Fourier coefficients after a discrete Fourier transform," *IEEE Trans. Instrum. Meas.* **IM-35**, 278–286 (1986).
21. M. Frank et al., "Theoretical and experimental error analysis of continuous-wave time-of-flight range cameras," *Opt. Eng.* **48**(1), 013602 (2009).
22. A. P. P. Jongenelen, "Development of a compact, configurable, real-time range imaging system," PhD Thesis, Victoria University of Wellington, New Zealand (2011).
23. S. Fuchs, "Multipath interference compensation in time-of-flight camera images," in *20th Int. Conf. on Pattern Recognition (ICPR)*, pp. 3583–3586 (2010).
24. M. Lindner et al., "Time-of-flight sensor calibration for accurate range sensing," *Comput. Vision Image Understanding* **114**(12), 1318–1328 (2010).
25. D. D. Lichti et al., "New models for scattering bias compensation in time-of-flight range camera self-calibration," *J. Surv. Eng.* **140**(2), 04014003 (2014).

Refael Whyte is a PhD student at the University of Waikato. He received his BE (hons) degree in electronic engineering from the University of Waikato in 2010. His research focus has been on resolving measurement errors present in time of flight range cameras.

Lee Streeter is a teaching fellow at the University of Waikato, Hamilton, New Zealand. He has an undergraduate background in physics and received his PhD from University of Waikato in 2010. In 2015 he was awarded the Fast Start grant by the Marsden Fund Council of the Royal Society of New Zealand to begin early 2016. His current research interests includes the metrology of time-of-flight range imaging to improve camera performance.

Michael J. Cree received his PhD in electrical and electronic engineering at the University of Canterbury, New Zealand, in 1994. After almost three years as a researcher at the University of Aberdeen, Scotland, he took up a position at the University of Waikato, New Zealand, where he is now senior lecturer in the Department of Engineering. His research interests include medical imaging, range imaging, and image processing.

Adrian A. Dorrington was awarded his PhD in 2001 from the University of Waikato, in Hamilton, New Zealand, and is currently a cofounder and CTO at Chronoptics Limited. He was previously a senior lecturer at the University of Waikato, where he founded and managed the Time-of-Flight Imaging Research Group and has held postdoctoral fellowships at the same university and at the NASA Langley Research Center. His research interests are in improving the capability of time-of-flight imaging.